Int. J. Electrochem. Sci., 10 **(2015)** 4946 - 4971

International Journal of
ELECTROCHEMICAL
SCIENCE
www.electrochemsci.org

Role of Glycine as a Complexing Agent in Nickel Electrodeposition from Acidic Sulphate Bath

Magdy A.M.Ibrahim[1,2,*] *and Rasha M. Al Radadi*[1]

[1]Chemistry Department, Faculty of Science, Taibah University, Al Maddinah Al Mounwara, 30002 KSA
[2]Chemistry Department, Faculty of Science, Ain Shams University, Abbassia, Cairo, 11566 Egypt
[*]E-mail: imagdy1963@hotmail.com

Received: 12 December 2014 / *Accepted:* 19 March 2015 / *Published:* 28 April 2015

Bright nickel coatings on copper substrates were successfully produced by electrodeposition using acidic glycine complexing baths. The investigation was conducted using electronic spectroscopy, potentiodynamic cathodic polarization, cyclic voltammetry, in situ-anodic linear stripping voltammetry and chronoamperometry techniques complemented with XRD analysis and SEM measurements. Such kinetic parameters as Tafel slope, transfer coefficient and exchange current density obtained from Tafel plots indicated that glycine had an accelerating effect on Ni^{2+} electroreduction. In the glycine-containing bath, SEM analysis revealed finer grains together with the appearance of fine microcracks. The XRD analysis showed an increase in noncrystallinity with increasing glycine concentration. The initial nucleation and growth of nickel followed the model of 3D instantaneous nucleation. The corrosion behaviour of the nickel coatings was studied using both anodic potentiodynamic polarization and open circuit potential tests in 3.5% NaCl solution, and the results indicated that glycine decreased the corrosion resistance of nickel deposits. The throwing power, as well as the throwing index, in the presence of glycine is lower than that observed in the absence of glycine.

Keywords: glycine; potentiodynamic polarization; complexes; SEM.

1. INTRODUCTION

Electrodeposition of nickel has been investigated extensively due to its particular mechanical properties and numerous widespread applications in industry [1–3], the majority of which require corrosion and heat resistance [4]. As highly resistant to tarnish and due to their high value of hardness, they have become an alternative for electroplated chromium in hardware, automotive, electrical and electronics accessories. Moreover, because of favourable mechanical properties, nickel electrodeposits

are used for electroforming of printing plates, phonograph record stampers, foil, tubes, screens and many other articles [5]. The selection of an electroplating bath depends primarily on the required characteristics. Electrodeposition of nickel has therefore been studied by various authors using different baths [6-10]. Also, nickel electroplates are extensively studied from Watts type baths in the presence of different organic brighteners [11-13]. On the other hand, glycine is used effectively in the electrodeposition of metals and alloys due to its high buffering properties and its ability to stabilises the pH on the electrode surface during the electrodeposition process [6,7,14-20]. Plating baths containing glycine have better current efficiency and lead to amorphous films compared to the crystalline films obtained using citrate [21]. Finally, glycine baths are more environment friendly than traditional cyanide baths. Few studies have been conducted on the electrodeposition of nickel from acidic glycine baths. Moreover, published data on the influence of glycine on the kinetics of electrode reactions during nickel electrodeposition are scarce. The present work aims to develop new baths for producing good quality nickel deposits. In addition, the investigation aims to elucidate the mechanism and kinetics of nickel electrodeposition from acidic glycine baths. The corrosion resistance of the nickel deposited as well as the throwing power and throwing index in the presence of glycine were also investigated.

2. EXPERIMENTAL

Nickel electrodeposition onto copper substrates was achieved using an acid sulphate bath containing $NiSO_4\,6H_2O$ and H_3BO_3 in the presence and absence of glycine as a complexing agent. All solutions were freshly prepared with distilled water and analytical grade reagents. The pH was adjusted using 1:1 sulphuric acid (sp.gr.1.84 g/cm^3) or potassium hydroxide (10% w/v) and was measured using a Janway 3540 pH meter. For nickel electrodeposition, a copper and a platinum sheets each of dimensions (2.5 x 2.5 cm) were used as cathode and anode respectively. The electrodeposition cell used was in the form of rectangular trough made of Perspex (11 x 3 cm) provided with vertical grooves on each of the side walls to fix the electrodes. Before each run, the copper substrate was cleaned by being dipped in a pickling solution for one minute and being rinsed in distilled water before being dried and weighed. Direct current was supplied by a DC power supply unit (QJ3005A). The determination of the cathodic current efficiency (F%) of nickel deposition was performed with a Cu coulometer and the equation ($F = W_{exp} / W_{theo}$), where W_{exp} is the weight of the deposit obtained experimentally, and W_{theo} is the weight of the deposit calculated theoretically according to Faraday's law [22]. All experiments were performed using unstirred solutions, 10 min plating duration, at a temperature of 20 ± 2°C. The TP% of the solution was measured using a Haring–Blum rectangular Perspex cell fitted with one anode between two parallel copper cathodes where the ratio of the far to the near distance was 5:1. The TP% was calculated from Field's formula [23]:

$$TP\% = (L - M) / (L + M - 2) \times 100 \quad (1)$$

Where, L is the ratio of the cathode distance to the anode distance (far to near 5:1), and M is the ratio of the weight of the deposited metal on the near to the weight of the deposited metal on the far cathode. The values of M were measured as a function of L over a wide range of linear ratios varying

between 1:1 and 5:1. The throwing index (TI) was considered to be the reciprocal of the slope of the M against L plot.

Potentiodynamic cathodic polarization curves were recorded using copper substrates by sweeping the potential from the rest potential toward the negative direction with a scan rate of 10 mVs^{-1}. All of the electrochemical experiments were carried out using a computer assisted potentistat/galvanostat (SI 1287 Solartron). The software packages CorrWare 2 and CorrView 2 provided by Solartron were used to measure and analyse the data. All potentials were measured relative to a saturated calomel electrode (SCE). The classic three-electrode cell was used for the cyclic voltammetry measurements. The working electrode was a glassy carbon electrode (GCE) (area = 0.1963 cm^2) enclosed in a PVC cylinder. The GCE was polished before each experiment with a diamond paste until a bright surface finishing was produced, then washed with distilled water. The counter-electrode was a platinum net. In the anodic linear stripping voltammetry measurements, the deposition of nickel from the plating bath was carried out at a constant potential at the GCE for a constant plating time. At the end of each deposition time, stripping analysis was performed immediately in the same plating bath (i.e., in situ) by sweeping the potential to more anodic potentials at a sweep rate of 10 mVs^{-1} [5,24]. The electrochemical corrosion tests were carried out using a classical three-electrode cell with platinum as the counter electrode, saturated calomel electrode as the reference electrode, and the samples with an exposed area of 1 cm^2 as the working electrode. The corrosive medium used for electrochemical corrosion tests was a neutral 3.5% NaCl solution, and the test temperature was maintained at 20°C. The surface morphologies of the nickel coatings was studied using a scanning electron microscopy (Model Philips XL-40 FEG). The phase and the crystal structure of the nickel coatings was analyzed by a Shimadzu XRD-6000 diffractometer (40 kV, 30 mA), Ni filter and CuKα radiation. The drive axis is theta-2theta, scan speed 2 deg/min and preset time 0.60 sec. The absorption spectra of nickel solutions at different pH values were measured by UV-Visible spectrometer (GBC UV-Visible Cintra 6). UV spectra were obtained using plastic cell with a light path length of 1.0 cm.

3. RESULTS AND DISCCUSION

Although glycine is usually presented as (H_2N-CH_2-COOH), it is considered as a dipolar ion (zwitterion) whose structure protonates or deprotonates, depending on the pH of solution [25]. The equilibria between these may be depicted as shown in equation (2). Therefore, complex equilibria take place in the solution are shown below [7,26].

$$\underset{\text{(anionic, } Gly^-\text{)}}{H_2N\text{-}CH_2\text{-}COO^-} \overset{H^+}{\underset{OH^-}{\rightleftharpoons}} \underset{\text{(dipolar, } HGly^{\pm}\text{)}}{{}^+H_3N\text{-}CH_2\text{-}COO^-} \overset{H^+}{\underset{OH^-}{\rightleftharpoons}} \underset{\text{(cationic, } H_2Gly^+\text{)}}{{}^+H_3N\text{-}CH_2\text{-}COOH} \qquad (2)$$

In the pH range from 3.0 to 8.0, nickel complexes of different compositions are detected in solution depending on the concentration ratio of Ni^{2+} to glycine ratio in the electrolytic bath. At still

higher pH values (8-10), Ni^{2+} exists preferentially as $[NiGly_3]^-$ which has the higher stability constant [7] as follows:

$$Ni^{2+} + Gly^- \rightleftharpoons [NiGly]^+ \qquad Log\ K = 5.87 \qquad (3)$$

$$Ni^{2+} + 2Gly^- \rightleftharpoons [NiGly_2] \qquad Log\ K = 10.54 \qquad (4)$$

$$Ni^{2+} + 3Gly^- \rightleftharpoons [NiGly_3]^- \qquad LogK = 14.26 \qquad (5)$$

$$H^+ + Gly^- \rightleftharpoons HGly \qquad Log\ K = 9.72 \qquad (6)$$

$$H^+ + HGly \rightleftharpoons H_2Gly^+ \qquad Log\ K = 2.56 \qquad (7)$$

Therefore, $[NiGly_3]^-$ is the most predominant complex species in the solution because it has a much higher equilibrium constant. In addition, because there are more Ni^{2+} ions than glycine, there will also be significant amounts of free Ni^{2+} ions present in the solution. Therefore, the following electroreduction reactions are possible with hydrogen evolution from independent side reactions:

$$Ni^{2+} + 2e^- = Ni \qquad (8)$$

$$[NiGly_3]^- + 2e^- = Ni + 3NH_2CH_2COO^- \qquad (9)$$

3.1 Absorption spectra

A change was observed in the colour of the nickel solutions as a function of the pH. This finding prompted a spectroscopic investigation in the visible region. This change may be due to transitions between the d orbitals of the transition metal in the coordination compounds.

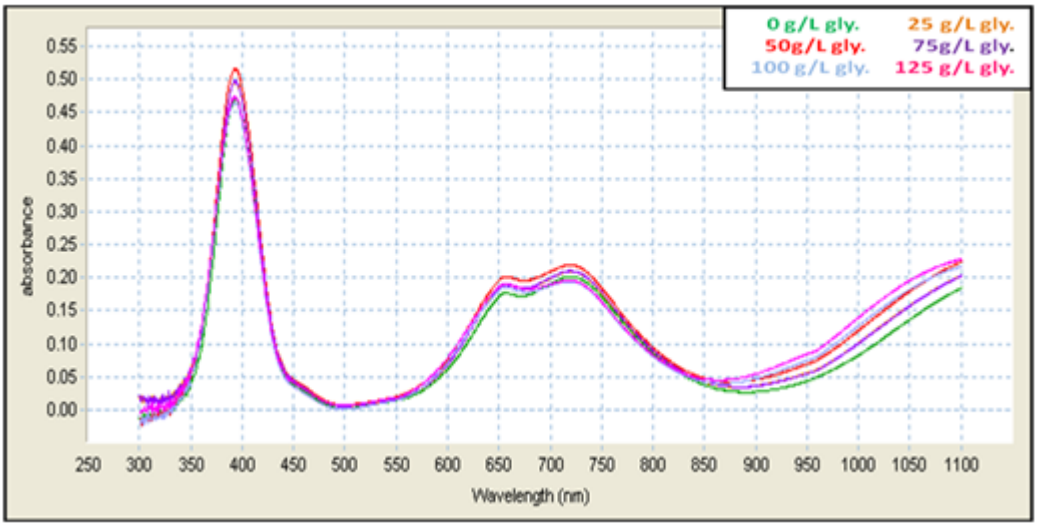

Figure 1. The absorption spectrum of a nickel solution containing: 100 g/L $NiSO_4$, 30 g/L H_3BO_3 at different concentration of glycine.

Fig. 1 illustrates the absorption spectra of nickel solutions at different concentrations of glycine in the wavelength range of 300 - 1100 nm at room temperature. The spectra show the appearance of one sharp transition at 385 nm and two transitions at 650 and 725 nm respectively due to the n-π* and d-d transitions, confirming the complex formation. It is also clear that the absorption spectra are independent on the glycine concentration in the electrolytic solution.

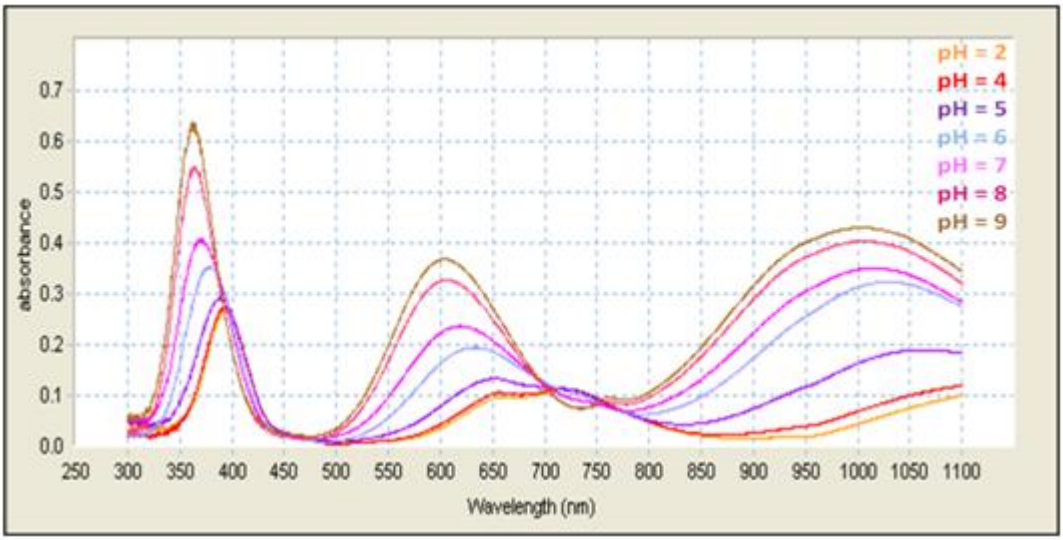

Figure 2. The absorption spectrum of a nickel solution containing: 100 g/L $NiSO_4$, 30 g/L H_3BO_3 and 100 g/L glycine at different pH values.

Fig. 2 shows the absorption spectra of Ni^{2+}- g1ycine solutions at different pH values. In this case, the two transitions at 650 and 725 nm are shifted to lower wavelengths and overlapped to one band at 600 nm at pH 9.0. Also, the n-π* transition is shifted to lower wavelengths by increasing the pH. This could be due to the change in the ratio of the complex from 1:1 to 1:3 complexes. Significant increase in the intensity of the absorption band can be noticed in going from low to high pH. This indicates that the formation of the Ni^{2+}-glycinate complex depends strongly on the pH. The formation of Ni^{2+}- glycinate complex is easier at higher pH than at lower pH, since the intensity of the absorption band of the Ni^{2+}-glycinate solution is stronger at high pH values. As the acidity of solution decreases and hence the amount of unprotonated glycine increases, the intensity of the bands grows which confirms the formation of a complex species. This result is consistent with the results obtained by Mizushima et al., [27].

3.2. Voltammetric behavior

3.2.1. Potentiodynamic cathodic polarization curves

Fig. 3 shows typical cathodic polarization (i/E) curves during nickel deposition onto copper substrate in the absence and presence of glycine (25-125 g/L). The curves were swept from the rest

potential (-0.4 V) towards the negative direction at scan rate of 10 mVs^{-1}. Discharge of hydrogen ions was observed simultaneously during the deposition of Ni^{2+} ions. The data show that the presence of glycine led to a significant shift in the polarization curves in the direction of more positive potentials in addition to the increase in the current density. This effect of glycine could be related to its complex formation with Ni^{2+} ions and it indicates that the complex formed activates the electroreduction of Ni^{2+} ions. This implies also that glycine acts as an accelerator for nickel reduction over the copper surface and does not block the active sites on the electrode surface for nickel deposition. This acceleration effect of nickel ions reduction in presence of glycine was also observed by Sotskaya et al., [7].

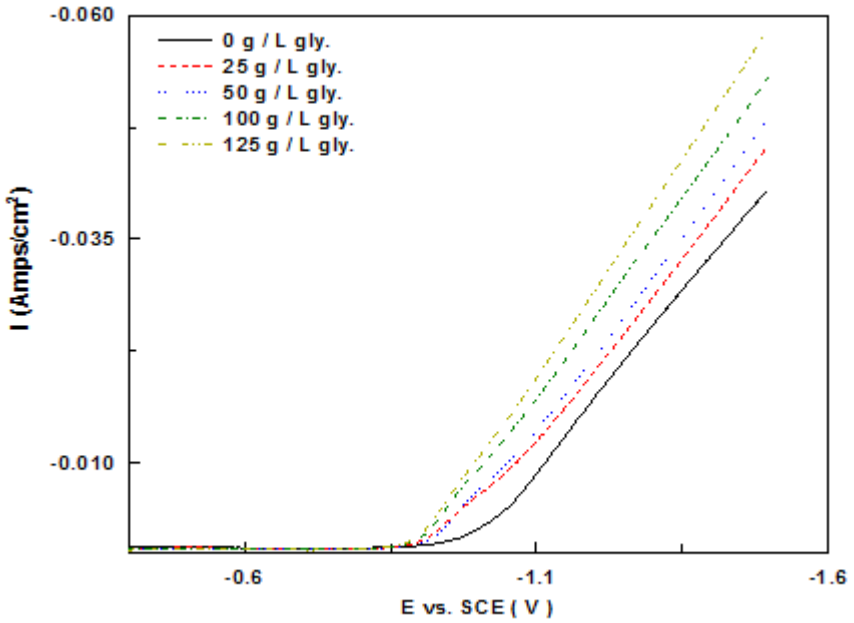

Figure 3. Potentiodynamic cathodic polarization curves during nickel deposition at different concentrations of glycine, scan rate = 10 mVs^{-1}.

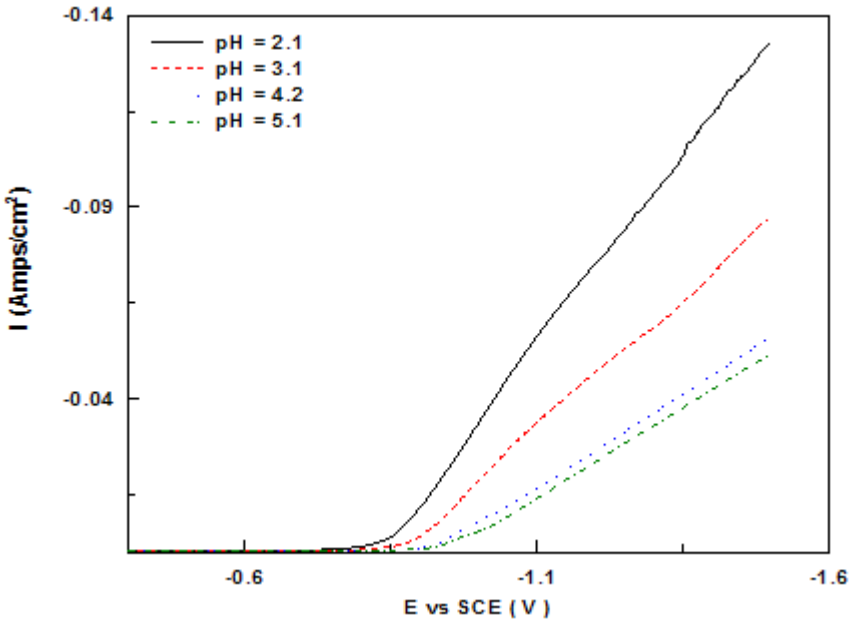

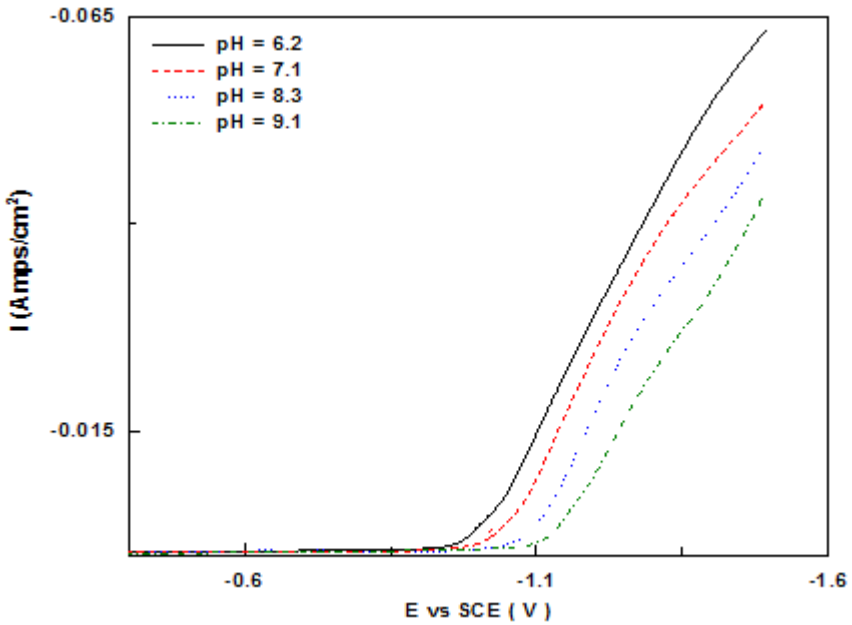

Figure 4. Potentiodynamic cathodic polarization curves during nickel deposition at different pH values, scan rate = 10 mVs^{-1}.

Fig. 4 (A and B) display the influence of pH (pH 2.1 – 9.1) on the cathodic polarization curves during nickel electrodeposition. The pH of each bath was adjusted by adding concentrated H_2SO_4 or KOH solution. The potentiodynamic cathodic polarization curve is shifted significantly negatively with increasing pH. Moreover, the deposition potential of nickel is occurred at high negative potential with increasing the pH. This trend may be related to the fact that increasing pH leads to an increase of the hydrogen ion dissociation from the glycine molecule. Thus, the concentration of free Ni^{2+} ions decreases as the pH increases. A consequent lowering of free Ni^{2+} ions results in a shift of the cathodic potentials to more negative values. It is worth mentioning that the polarization curve at pH 2.1 is mainly due to the hydrogen discharge at the cathode. With increasing pH, the slope of the i-E curves increases as a result of a high rate of simultaneous hydrogen evolution with nickel deposition.

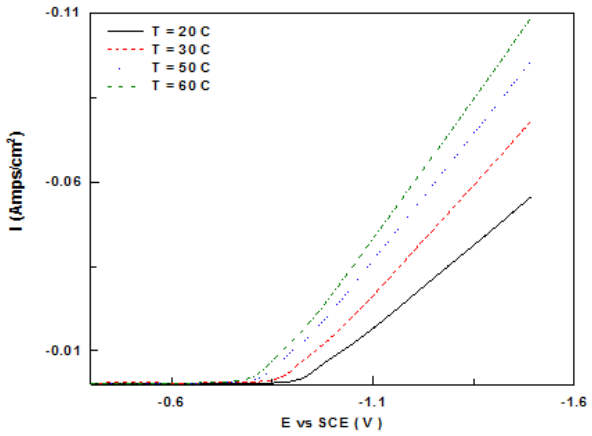

Figure 5. Potentiodynamic cathodic polarization curves during nickel deposition at different temperatures, scan rate = 10 mVs^{-1}.

The effect of bath temperature on the potentiodynamic cathodic polarization curves during nickel deposition is shown in Fig. 5. An increase in bath temperature decreases the cathodic polarization due to its effect on the activation overpotential for the reducible ions. Moreover, an increase in temperature may change the relative abundance of both complexed and uncomplexed Ni^{2+} ions in the solution. These results indicate that a rise in temperature favours the complex ion dissociation. Consequently, the concentration of the uncomplexed Co^{2+} ions would result in a decrease in the reduction overpotential.

3.2.1.1.Tafel lines and electrode kinetics

To investigate the kinetics of nickel deposition in the presence of glycine, Tafel lines were used to calculate the electrochemical parameters such as the Tafel slope b_c and the transfer coefficient α. The exchange current densities i_o for nickel deposition were obtained by extrapolating the Tafel lines to zero overpotential which give relative rates of reaction at equilibrium. The data indicate that the Tafel slopes increase in the presence of glycine and it increases with increasing the glycine concentration in the bath. On the other hand, the transfer coefficient α decreases with increasing glycine concentration, implying that the charge transfer reaction is affected by the presence of glycine (Table 1)**.** Moreover, the exchange current density, i_o, is markedly increased with increasing glycine concentration. Generally, the exchange current density i_o is increased when the electrochemical reaction is accelerated [28]. This finding implies that glycine accelerates the rate of Ni^{2+} ion transfer across the electrical double layer. The accelerating effect of glycine could be due to its complex formation with Ni^{2+} ions, which activates the electroreduction of Ni^{2+} ions.

On the other hand, the effect of changing the pH values shows that the Tafel slope are high at low pH values as a result of hydrogen overvoltage and low at high pH. At the same time the exchange current density significantly decreases while the transfer coefficient increases. In contrast, raising the bath temperature, results in an increase in both the Tafel slope and i_o and a slight decrease in the transfer coefficient. The increase in i_o may be attributed to the fact that a rise in temperature favours the complex ion dissociation, as mentioned before. Consequently, the concentration of the free Ni^{2+} ions would increase and the reduction of Ni^{2+} ions occurs more readily.

Table 1. Tafel kinetic parameters obtained for nickel deposit in absence and presence of glycine at different deposition conditions.

Variable	$i_\circ$ (A cm^{-2})	α_c	$-b_c$ (mV $decade^{-1}$)
[glycine] , g/ L			
0	5.76×10^{-4}	0.09	323
25	5.89×10^{-4}	0.06	486
50	5.99×10^{-4}	0.06	502
100	6.65×10^{-4}	0.05	533
125	7.61×10^{-4}	0.05	562

Temp. /^{o}C			
20	3.92 x 10^{-4}	0.06	487
30	1.05 x 10^{-3}	0.05	554
50	5.81 x 10^{-3}	0.05	664
60	6.04 x 10^{-3}	0.05	685
pH			
2.1	1.19 x 10^{-2}	0.04	740
3.1	6.66 x 10^{-3}	0.05	634
4.2	4.12 x 10^{-4}	0.06	493
5.1	2.28 x 10^{-4}	0.07	439
6.2	4.65 x 10^{-5}	0.09	315
7.1	1.24 x 10^{-6}	0.14	210
8.3	4.32 x 10^{-8}	0.18	163
9.1	1.78 x 10^{-8}	0.18	158

3.2.2 In situ-Anodic linear stripping voltammetry (ALSV)

ALSV is particularly useful as a simple and easy 'in situ' electrochemical method for identifying the phase and composition of metal and alloy. A series of voltammetric experiments was carried out by the deposition of nickel onto a glassy carbon electrode (GCE) at a given constant cathodic potential (-1.15 V_{SCE}) for a given time (100 s). Immediately after nickel deposition, the potential was swept linearly in the positive direction at a scan rate of 10 mVs^{-1} and an anodic stripping voltammogram was recorded without removing the electrode from the solution or changing the prevailing conditions.

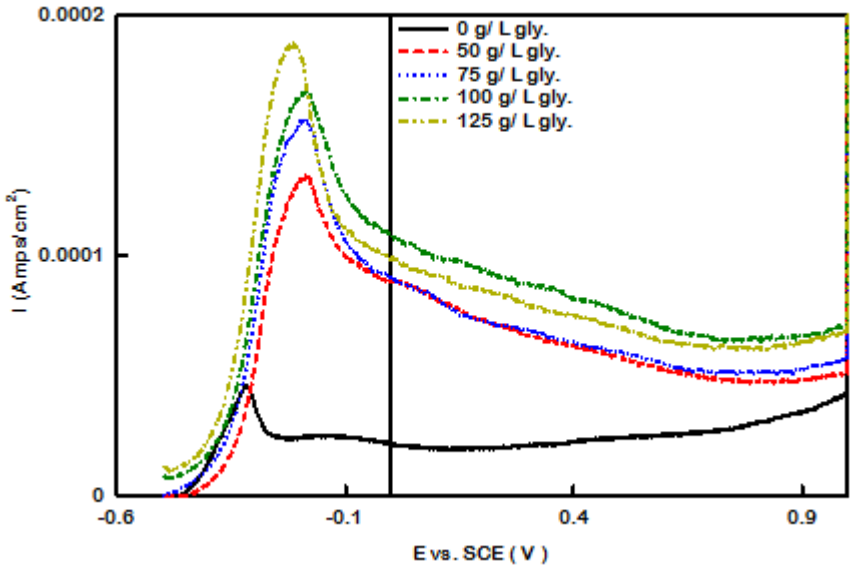

Figure 6. In-situ anodic linear stripping voltammetric curves during nickel deposition at different concentrations of glycine.

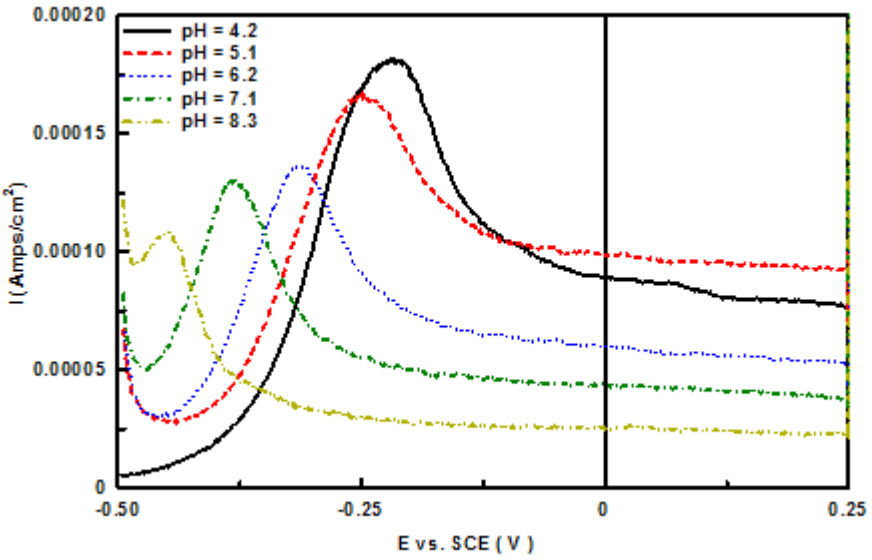

Figure 7. In-situ anodic linear stripping voltammetric curves during nickel deposition at different pH values.

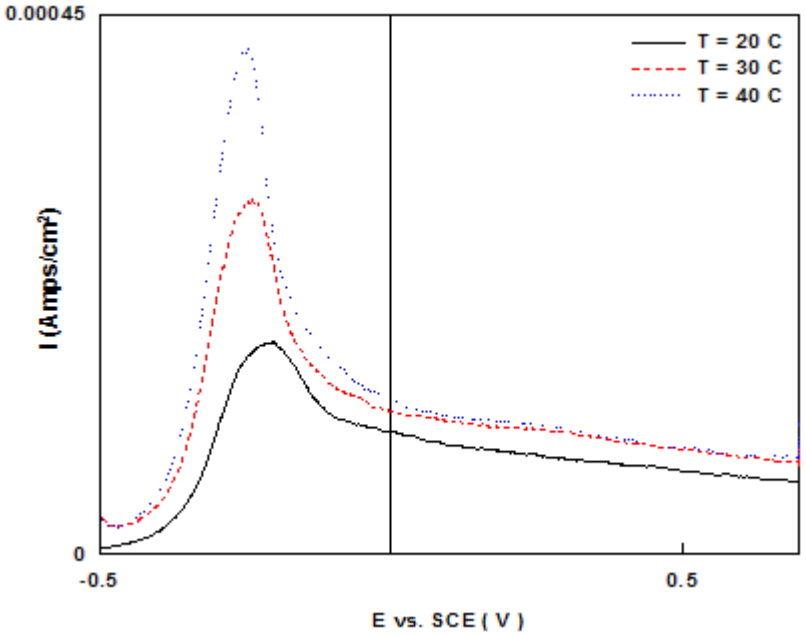

Figure 8. In-situ anodic linear stripping voltammetric curves during nickel deposition at different temperatures.

Representative data are given in Figs. 6 -8. The voltammograms of nickel in all cases studied has only one dissolution peak, which arises from dissolution of nickel deposited potentiostatically. No residual nickel or nickel oxide was visible on the GCE beyond the anodic peak. Therefore, the charge consumed through anodic stripping could be taken as a quantitative measure of the current efficiency of nickel deposition, i.e., the area under the peak is equivalent to the amount of nickel deposited.

The effect of adding different concentrations of glycine on the ALSV was studied and the results are shown in Fig. 6. It is clear that increasing the glycine concentration increases the height and the area under the stripping peak indicating clearly that glycine acts as an accelerator for nickel deposition. This acceleration process increases with increasing glycine concentrations. These results agree well with the data of the polarization curves (see Fig. 3). On the other hand, in the presence of glycine, the peak of ALSV lies at more positive potential indicating that the nickel deposited in the presence of glycine is difficult to oxidized in comparison with that deposited in absence of glycine.
Fig. 7 illustrates the ALSV curves during nickel electrodeposition at different pH values. Increasing the pH values resulted not only in a decrease in the height of the stripping peak but also in a decrease of the area under the peak. The results indicate that the stripping charge for nickel deposition decreases with increasing pH. These results also agree well with the polarization curves (Fig.4).

Fig. 8 shows the ALSV during nickel electrodeposition at different bath temperatures. The results indicate that the stripping charge for nickel deposition increases with increasing the bath temperature which indicates that a rise in bath temperature decreases the stability constant of the complex species leading to relatively higher concentrations of the uncomplexed Ni^{2+} ions.

3.2.3. Cyclic voltammetry

Cyclic voltammetry was used to determine the reduction potential regions for the characterisation of nickel deposition process. Figs. 9 and 10 show the voltammograms of Ni electrodeposition on GCE recorded at scan rate of 100 mVs^{-1}. In each voltammogram there is no difference in the oxidation wave during the anodic scan and that we have identified to study the change in reduction wave during the cathodic scan.

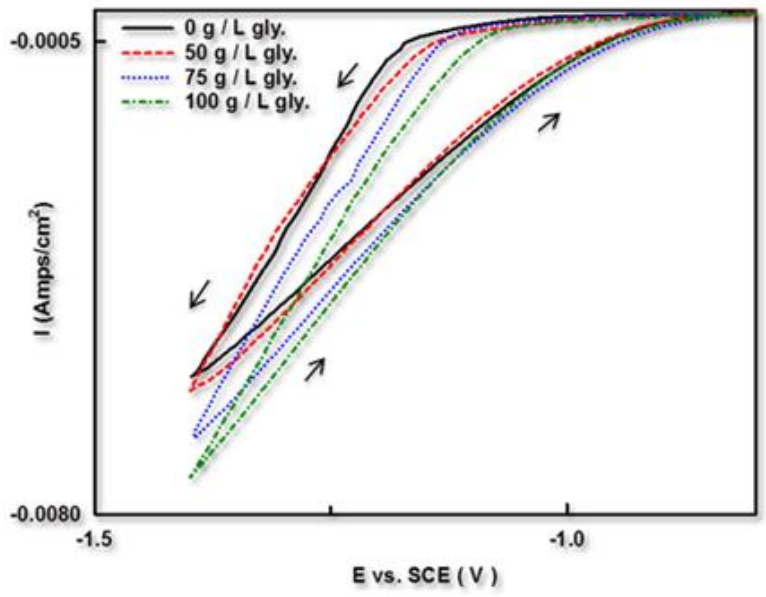

Figure 9. Cyclic voltammetric curves recorded at GCE during Ni deposition at different concentrations of glycine, scan rate = 100 mVs^{-1}.

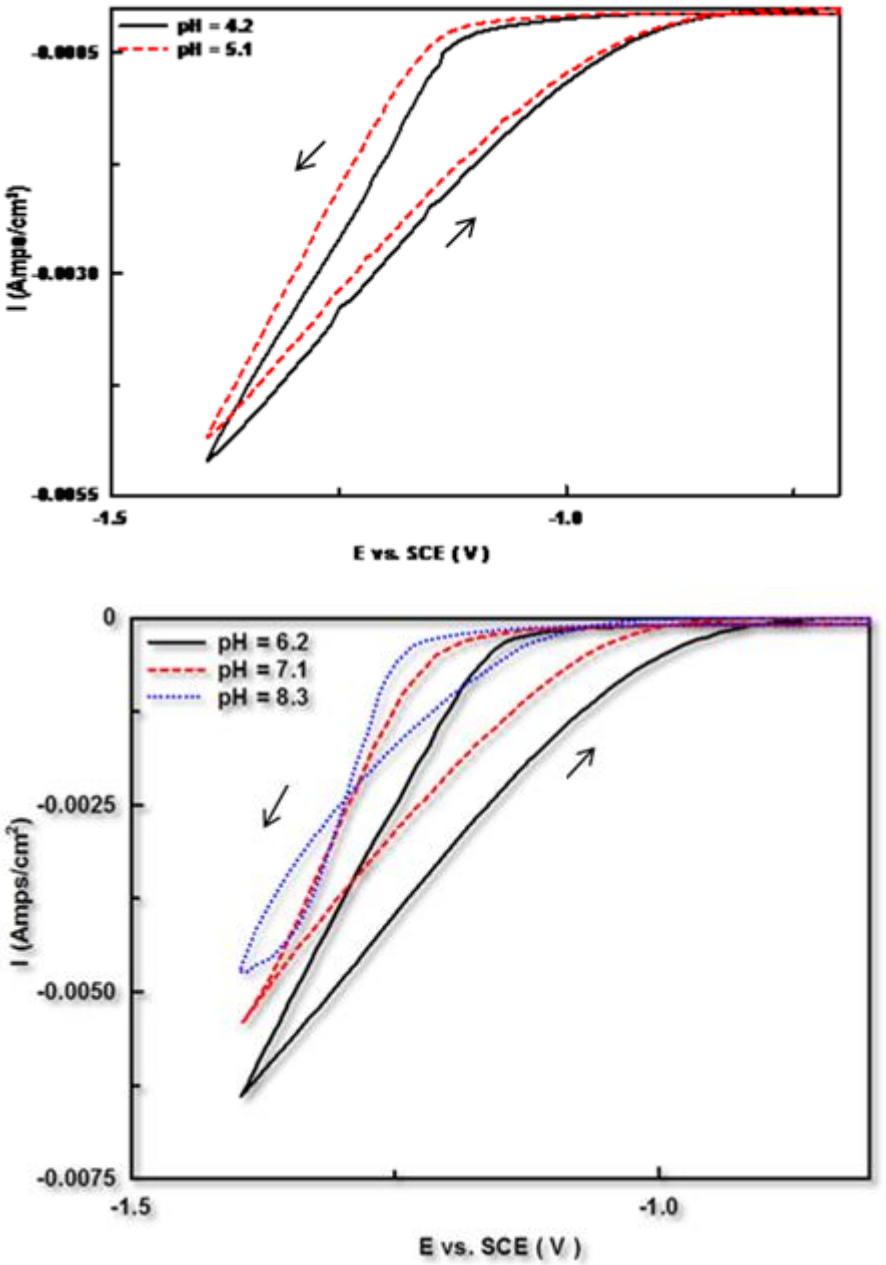

Figure 10. Cyclic voltammetric curves recorded at GCE during nickel electrodeposition at different pH values, scan rate =100 mVs^{-1}.

Fig. 9 shows the cyclic voltammograms of nickel deposition with various concentrations of glycine. In the presence of glycine, the potential of cathodic reduction of Ni^{2+} shifted to less negative potentials. This effect of glycine could be related to its complex formation with Ni^{2+} ions which indicates that the complex formed activates the electroreduction of Ni^{2+} ions. This implies that glycine acts as an accelerator for nickel deposition over the copper substrate and does not block the active sites on the electrode surface for nickel deposition. This result is consistent with the results of cathodic polarization curves **(**Fig. 3**)**.

The influence of pH on the cyclic voltammetry during nickel electrodeposition was examined and the results are shown in Fig. 10 A, B. It was found that the potential of cathodic reduction of nickel

is significantly shifted to more negative potential values with increasing the pH in agreement with the results of polarization curves shown in Fig. 4.

3.3. Cathodic current efficiency

Visual observation of nickel coatings deposited from glycine baths showed that the deposit has bright appearance all over the current densities studied and the electrolytes studied can be used to obtain bright nickel deposits without introduction of brightening additives.

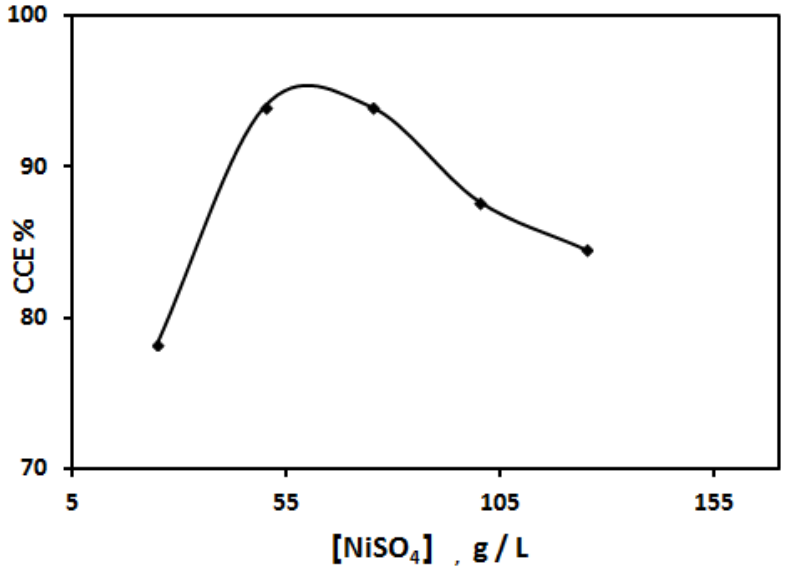

Figure 11. Effect of $NiSO_4$ concentration on the cathodic current efficiency during nickel deposition.

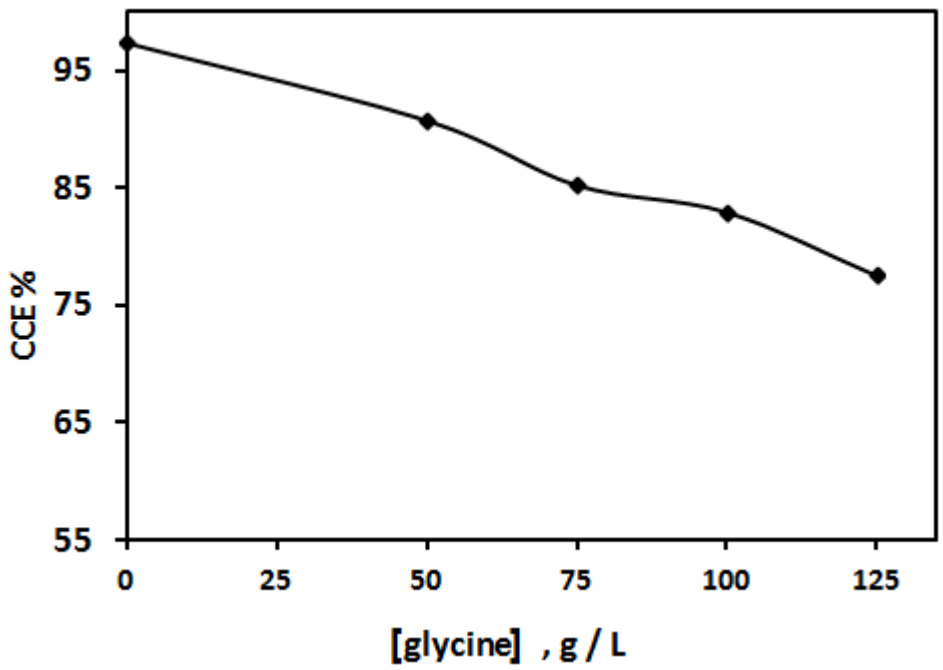

Figure 12. Effect of glycine concentrations on the cathodic current efficiency during Ni deposition.

Fig. 11 shows the effect of $NiSO_4$ concentrations (25-100 g/L) on the cathodic current efficiency (CCE%). The data show that, increasing Ni^{2+} content in the bath leads to a gradual increase in the CCE reached a maximum value of 93.9 % at 50 g/L, and then with further increase in nickel content in the bath, it decreases to reach 84.5% at 125 g/L. The CCE% determined from these baths is less than 100% as a result of simultaneous hydrogen evolution. Addition of glycine to the electrolytic bath decreases gradually the CCE% of nickel deposition as shown in Fig. 12.

This may be attributed to the fact that increasing the glycine concentration, increases the concentration of complex ions, and decreases the concentrations of uncomplexed Ni^{2+} ions, which in turn causes an increase of the cathodic overpotential and a lowering of cathodic current efficiency. The deposition from complex species is not so easy like the deposition from free Ni^{2+} ions [29].

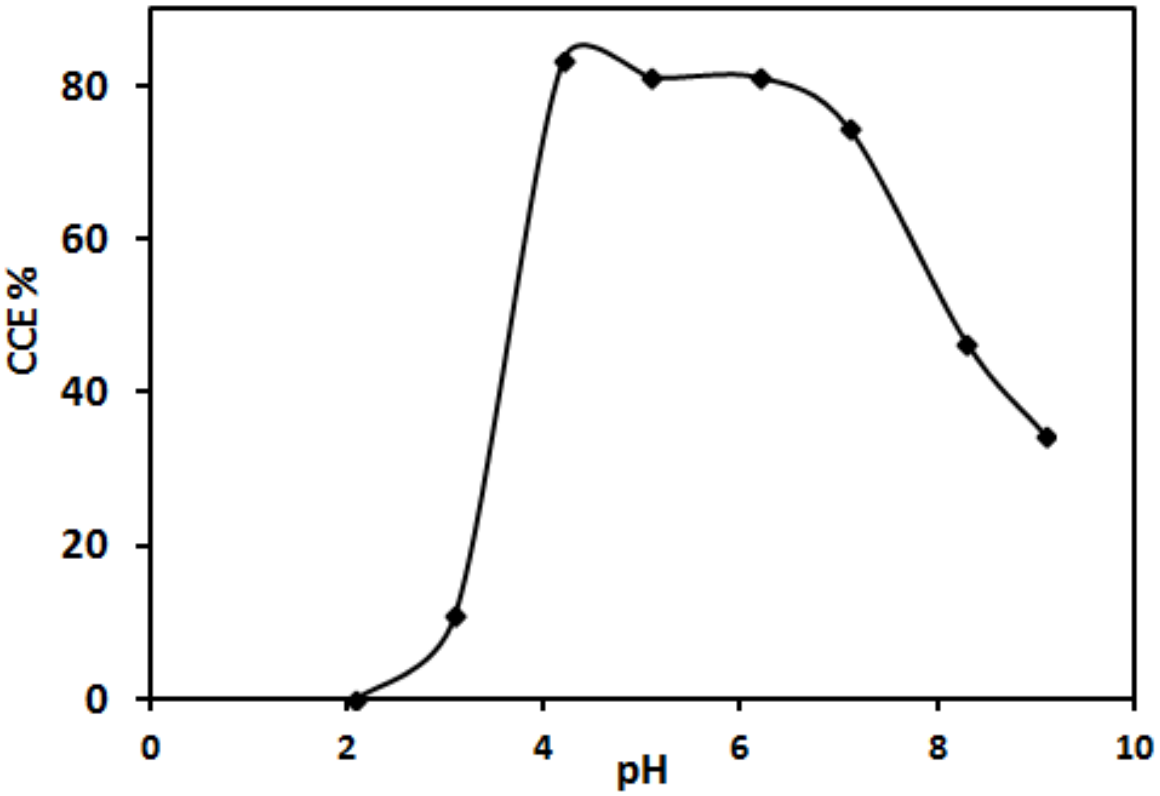

Figure 13. Effect of pH on the cathodic current efficiency.

One of the most important operating parameters in the electroplating process is the pH value. The data in Fig. 13 shows the influence of pH on the CCE% in the pH range from 2.1 to 9.1. The data indicate that the CCE% increases sharply reaching maximum values at pH between 4 and 7 and decreases with further increase in pH. The low values of CCE% for Ni deposition at low pH values could be due to the decrease in hydrogen overpotential and consequently the enhancement of hydrogen evolution reaction, although lowering pH increases the concentration of the free Ni^{2+} in the bath.

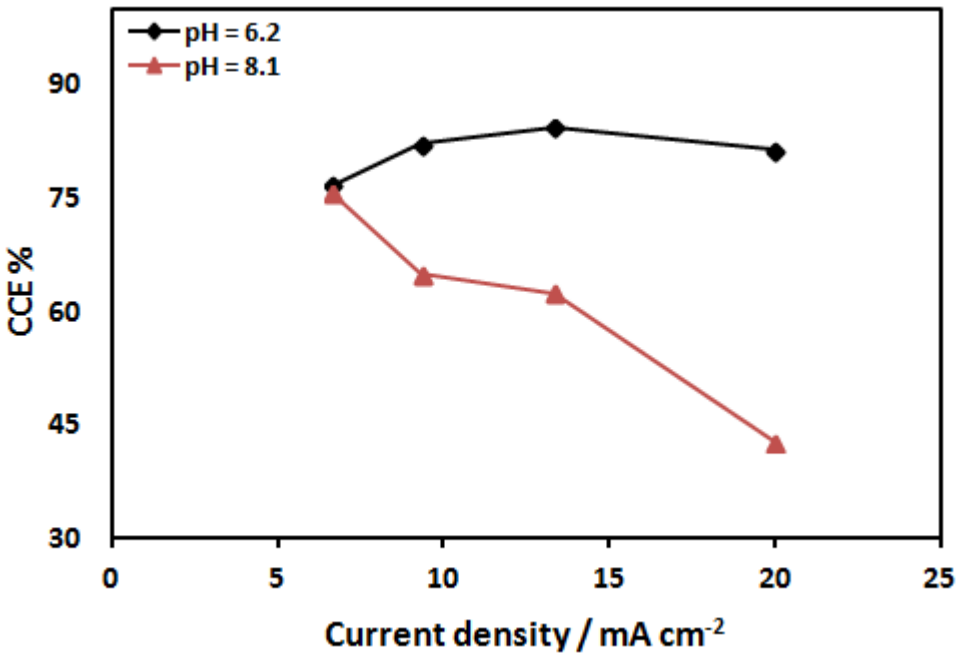

Figure 14. Effect of current density on the cathodic current efficiency at different pH.

The effect of current density on the CCE at two different pH values (pH 6.2 and pH 8.1) was studied and the results are given in Fig. 14. The data clearly reflect that the pH variation is still more pronounced than that of current density. For example, at pH 6.2, the CCE increases slightly with increasing current density and then tends to level off with further increase in the current density. However, at pH 8.1, a significant decrease in the CCE is observed with increasing current density.

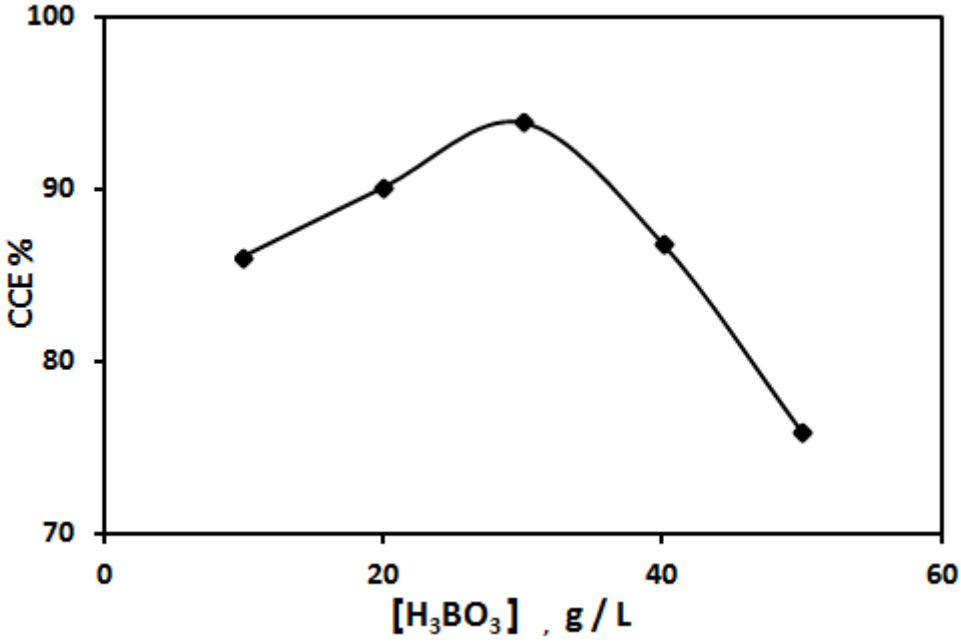

Figure 15. Effect of H_3BO_3 concentration on the cathodic current efficiency during Ni deposition.

The effect of boric acid concentration on the CCE% of nickel deposited is given in Fig. 15. The CCE incre ases from 86.1% to a maximum value of 93.9% with increasing boric acid concentration from 10 to 30 g/L. These data show that the presence of boric acid in the bath improves the efficiency of Ni deposition. In this case, boric acid plays a greater role than merely as a buffer. It is now believed that boric acid complexes with Ni^{2+} ions acting as a homogeneous catalyst or adsorbs on the electrode surface [30-32], which lowers the overpotential for nickel deposition. However, further increase in concentration of boric acid (> 30 g/L) has a decreasing effect on the CCE.

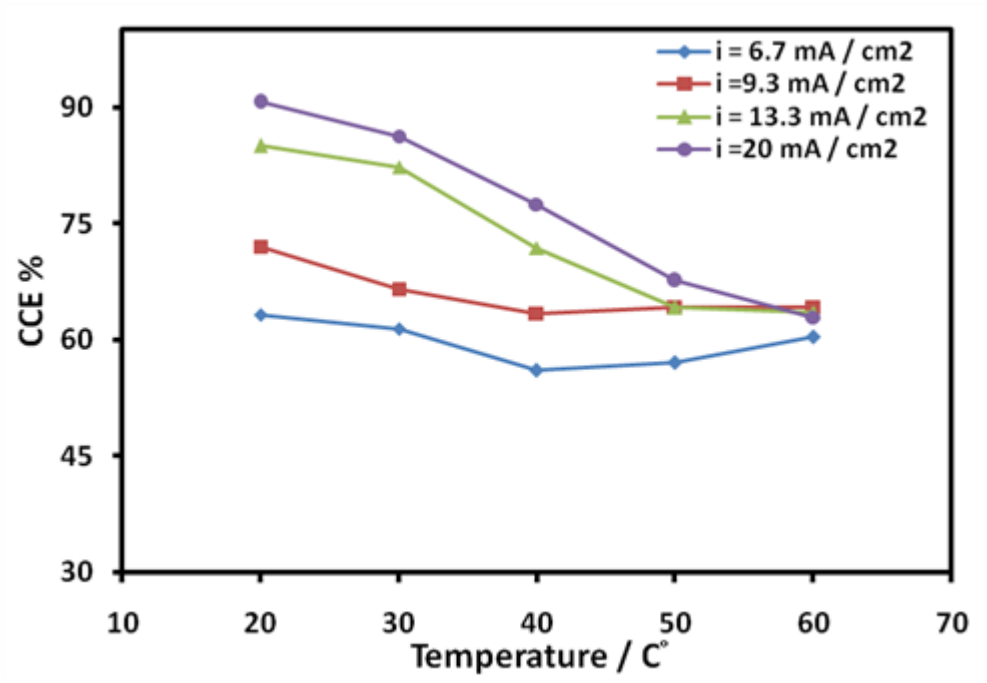

Figure 16. Effect of temperature on the cathodic current efficiency at different current densities.

The effect of bath temperature on the CCE% of nickel deposited at different current densities was studied and the results are shown in Fig. 16. The data indicate that at a given current density, the CCE decreased with increasing the bath temperature especially at high current densities of 13.3 and 20 $mAcm^{-2}$. However, at low current densities of 6.3 and 9.3 $mAcm^{-2}$, the CCE decreases slightly and then tends to level off. On other words, increasing bath temperature leads to a decrease in CCE and this effect is more pronounced at high current densities. Similar behavior was observed during cobalt electrodeposition from gluconate bath [33]. It is worth mentioning that, high efficiency at low temperature could be considered as an advantage in industrial applications.

3.4. Chronoamperometric analysis

Chronoamperometry (current –time transient) measurements were conducted at GCE to obtain more information about the initial nucleation and growth kinetic mechanism of nickel deposition in

glycine bath. Fig. 17 shows typical potentiostatic current time transients for nickel deposition from bath contains: 100 g/L $NiSO_4$, 30 g/L H_3BO_3 and 100 g/L glycine at various deposition potentials. During the potential step, the current-time transients are characterized by a graduall double-layer charging current decay [34] followed by a rising current due to the formation and growth of Ni nuclei. The current increases with increasing the applied nucleation overpotential. It has been demonstrated that the deposition of metals onto a foreign substrate generally involves some type of three dimensional nucleation processes. Two limiting cases for this type of metal deposition have been classified by Scharifker and co-workers[35-37] as instantaneous nucleation and progressive nucleation. The instantaneous model refers to the situation in which a fixed number of nucleation sites are all activated at the same time after the potential step, whereas progressive model refers to the situation in which the nucleation sites gradually become activated as the chronoamperometric experiment proceeds.

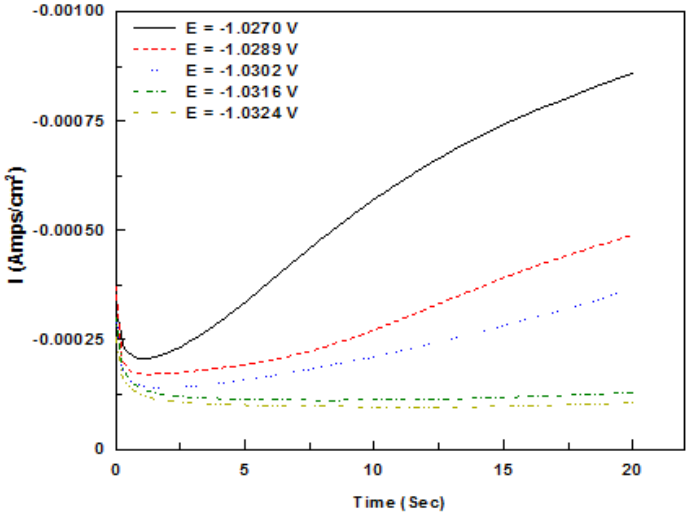

Figure 17. Potentiostatic current-time transient curves during nickel electrodeposition at different deposition potentials.

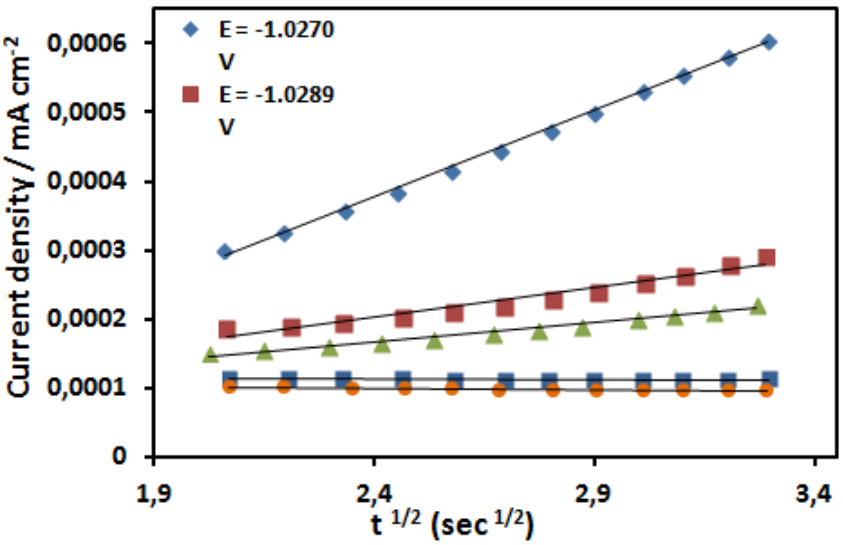

Figure 18. Relationship between the current density and $t^{1/2}$ during nickel electrodeposition derived from Fig.17 at different deposition potentials.

Analysis of the rising part of transient is possible by representing, for the initial transient portion, i vs $t^{1/2}$ for instantaneous and i vs $t^{3/2}$ for progressive nucleation. For the experimental data shown in Fig. 17, plots of i vs $t^{1/2}$ show good linearity (Fig. 18). On the other hand, plots of i vs $t^{3/2}$ show poor linearity. This indicates that under the experimental conditions, instantaneous three-dimensional growth of nickel nucleation occurs.

3.5. Throwing power, throwing index and Wagner number

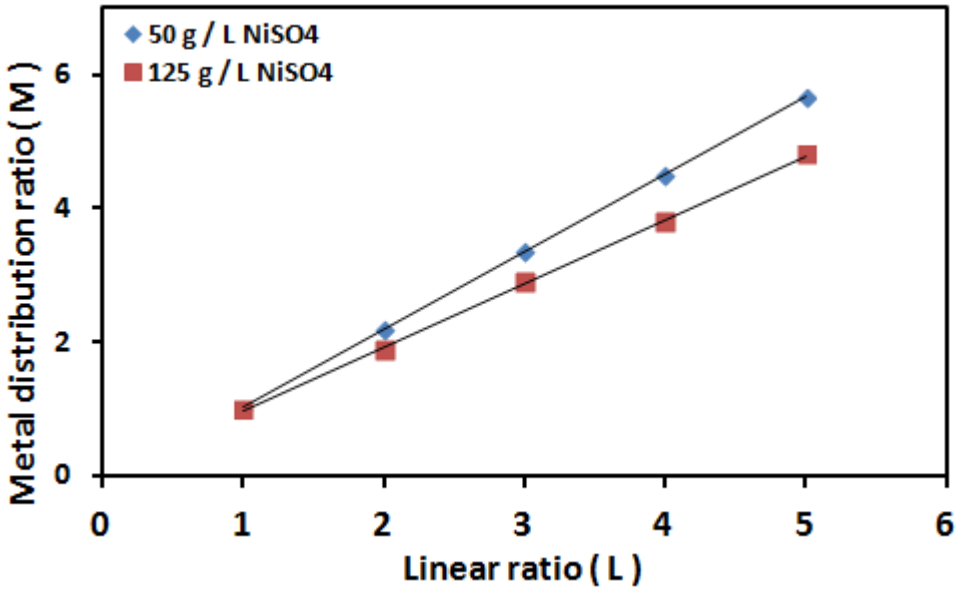

Figure 19. Metal distribution ratio M against linear ratio L at different $NiSO_4$ concentrations.

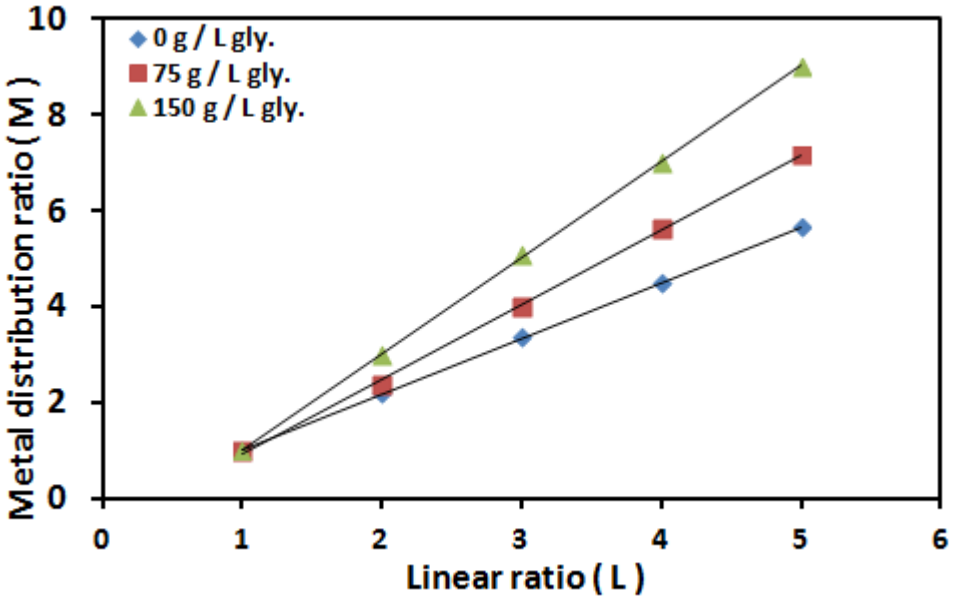

Figure 20. Metal distribution ratio M against linear ratio L at different glycine concentrations.

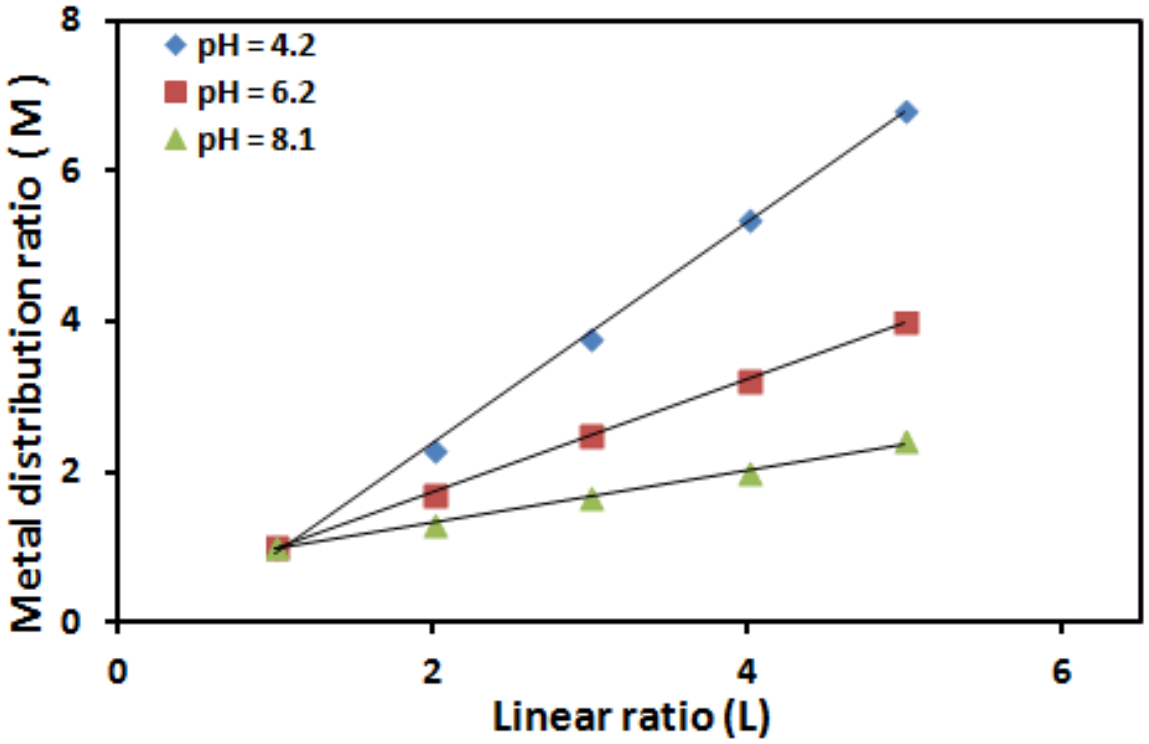

Figure 21. Metal distribution ratio M against linear ratio L at different pH values.

The throwing power values of the nickel plating baths calculated by Field's empirical formula at a distance ratio of 1:5 under different plating conditions are shown in Table 2. Moreover, the throwing index (TI) was determined by plotting the metal distribution ratio M, and the linear ratio L (1:1–1:5) as shown in Figs. 19-21 as representative examples. The reciprocal of the slopes of these lines are called the throwing index (TI) and represent a measure of bath throwing power.

Table 2 shows that the TP increases from -8.05% to 1.69 % as the nickel salt increases in the bath from 50 to 125 g /L. The corresponding TI values are 0.86 and 1.05 respectively as deduced from Fig. 19. The increase in TP is due to the observed increase in conductivity from 14.8 mS to 28.9 mS.

The data in Table 2 reveals that TP and TI decrease as the concentration of glycine increases (Fig. 20). This behavior could be assigned to the observed decrease in the cathodic polarization with increasing glycine concentration (Fig. 3).

The influence of pH on the TP and on TI was also investigated and the results are summarized in Table 2. Increasing pH value of the plating solution leads to a remarkable increase in TP and TI (Fig. 21). This improvement in TP may be attributed to the increase in the cathodic polarization as well as the conductivity with increasing pH (Fig. 4**)**.

The throwing power can be expressed by Wagner number (Wa). The degree of electrodeposition uniformity is characterized by the Wagner number Wa [38,39], which represents the ratio of the electrochemical reaction to the ohmic resistances. The Wa is used to characterise the relative importance of charge transfer control on the current distribution. The current distribution is expected to become more uniform as the Wa increases [40]. The Wa is defined by:

$$Wa = \frac{x}{k} \times \frac{d\eta}{di} \quad (10)$$

Where, k is the electrolyte conductivity of the solution, x is the breadth of the electrode (2.3 cm in this work), $\frac{d\eta}{di}$ is the slope of the potential-current density curve. The Wagner numbers calculated for different solutions are included in Table 2. The results confirm that the current density distribution becomes less uniform as the Wagner number decreases. The data of the throwing power, throwing index and Wagner number are in good agreement with each other. The less uniform the current distribution, the lower the Wagner number and consequently the lower the throwing power as well as the throwing index.

Table 2. Throwing power, throwing index and Wagner number for nickel electrodeposition

Variable	**TP**	**TI**	**Wa**
[$NiSO_4$**]**, g/L			
50	-8.05	0.86	-
125	1.69	1.05	-
[glycine**]**, g/L			
0	-8.05	0.86	3.47
75	-20.00	0.64	3.06
150	-34.21	0.50	2.21
pH			
4.2	-11.37	0.68	0.45
6.2	14.29	1.33	0.59
8.1	49.25	2.84	0.30

3.6. Characterization of nickel deposits

3.6.1. Surface morphology of nickel deposits

The surface morphology of the as-deposited nickel deposited from glycine-containing and glycine-free baths was examined by scanning electron microscopy (SEM) and the results are given in Fig. 22. The nickel deposited on copper substrate from glycine-free bath consists of grains of mud-like structure of different sizes as shown in Fig. 22 a. However, the addition of glycine to the plating solution (75 g / L) leads to the formation of fine and a homogenous circular grains but containing cracks as shown in Fig. 22b. These microcraks become larger with increasing glycine concentration (Fig. 22C). The presence of microcracks in the deposit indicates that the deposits are highly stressed as a result of hydrogen evolution during deposition [41]. The cracking occurs if the tensile stress exceeds the tensile strength of the film.

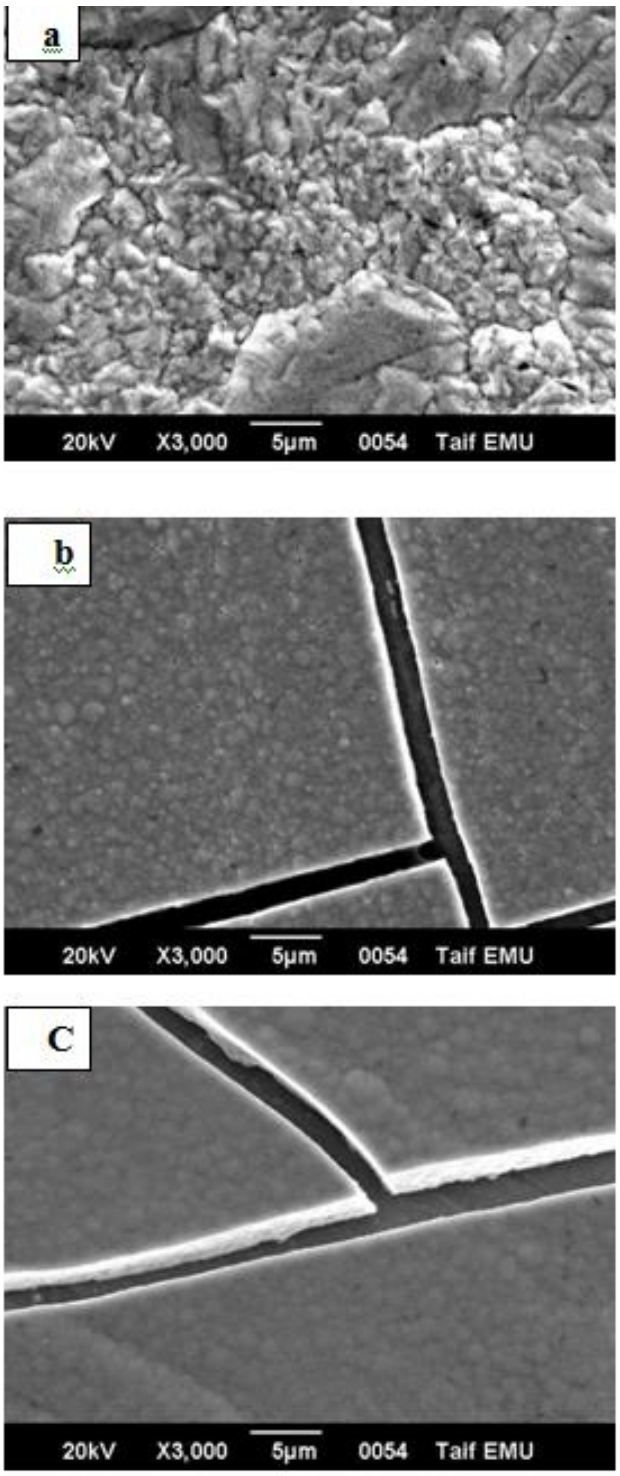

Figure 22. Photomicrograph of nickel deposited in the absence and presence of different glycine concentrations (a) 0 g/L glycine, (b) 75 g/L glycine, (c) 125 g/L glycine.

3.6.2. X-ray diffraction analysis

The XRD patterns of a typical Ni-deposited from glycine-containing and glycine-free baths are shown in Fig. 23.

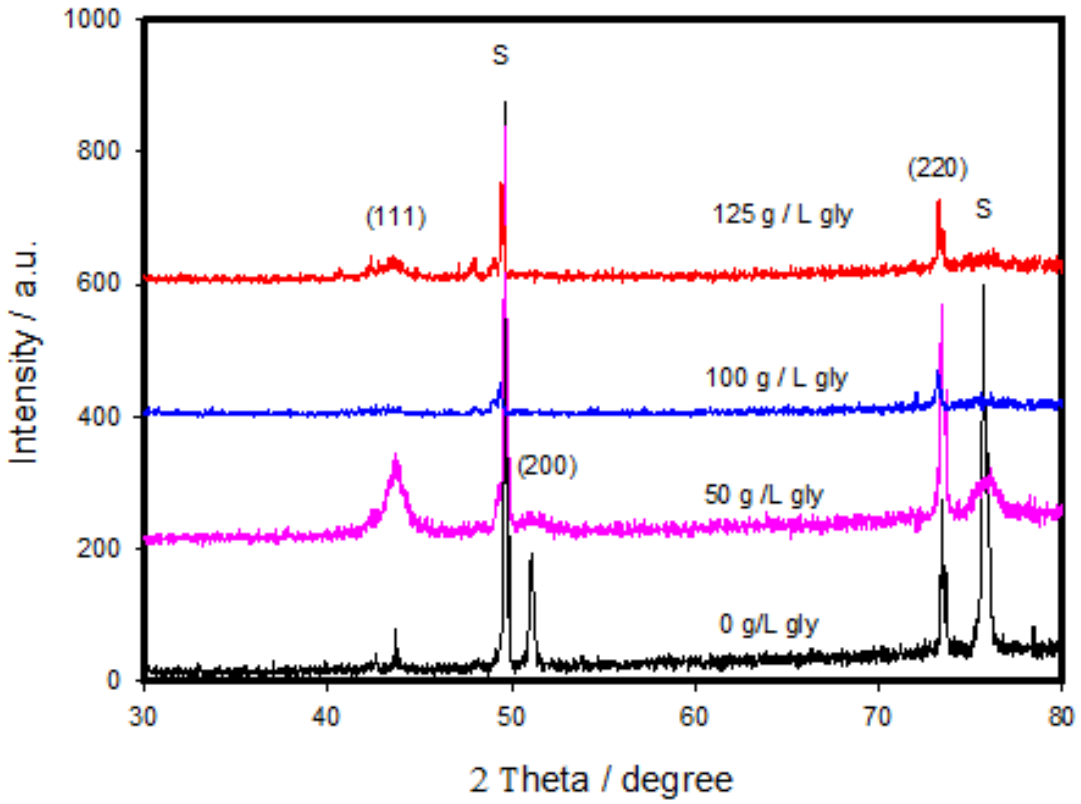

Figure 23. X-ray diffraction analysis of nickel deposited in the absence and presence of glycine, s is the substrate.

As shown in this figure, the Ni deposit in the absence of glycine exhibits three reflections at 2θ characteristic for Ni(200), Ni(220) and Ni(111), respectively. However, addition of 50 g /L glycine leads to retard the peak of Ni(200) and enhances the peak of Ni(111). Further increase in glycine concentrations shows clearly a decrease in crystallinty of nickel deposited. For example increasing the glycine concentration to be 100 or 125 g / L leads to decrease the degree of crystallinty as observed by the complete disappear of Ni(200) reflection and the decrease in Ni(220) intensity.

3.7. Corrosion behavior

3.7.1 Anodic potentiodynamic polarization curves

One of the most important properties of electrodeposited coatings is their corrosion resistance. Therefore, the corrosion behavior of the as-deposited nickel from glycine-containing and glycine-free baths was examined in 3.5% NaCl solution by means of anodic potentiodynamic polarization measurement.

Fig. 24 shows the anodic potentiodynamic polarization curves for nickel coating deposited on copper substrate in 3.5% NaCl. The curves were obtained by sweeping the potential starting from -2.0 V_{SCE} up to an anodic potential of 1.0 V_{SCE} at scan rate of 10 mVs^{-1}. As can be observed, all of the samples studied exhibited an active-passive – transpassive behavior. However, the nickel deposited

from glycine-free bath is characterized by wider range of passivity. The i_{corr} (corrosion current density) and E_{corr} (corrosion potential) which were calculated by using linear Tafel fitting on the anodic and cathodic Tafel regions of the potentiodynamic polarization curve are listed in Table 3. As can be observed the corrosion current i_{corr} increases and the E_{corr} is shifted to more negative potential values, in cases of samples prepared from glycine-containing baths. This result indicates that the Ni coating glycine-free solution has a higher corrosion resistance relative to Ni coating from glycine-containing solution, which corresponds to an increase of the corrosion rate of nickel.

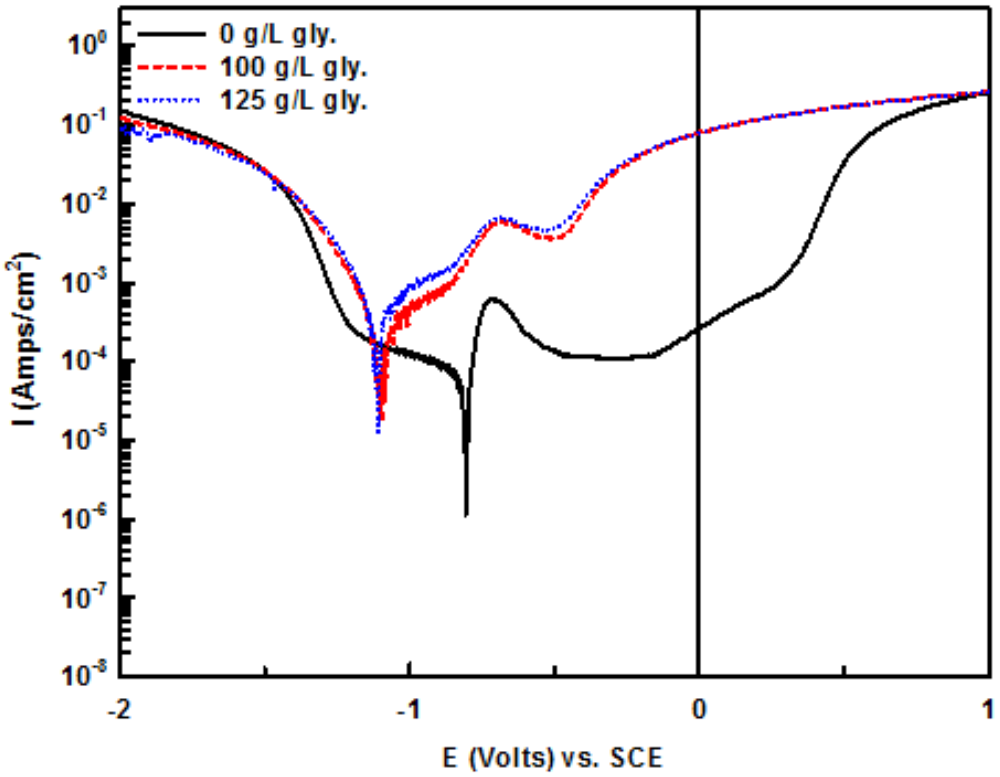

Figure 24. Anodic potentiodynamic polarization curves for nickel deposited in the absence and presence of different concentrations of glycine in 3.5% NaCl.

Table 3. Electrochemical parameters of nickel deposits at different glycine concentrations.

[glycine] g/ L	I_{corr} (Acm^{-2})	E_{corr} (volts)
0	0.00014333	-0.80574
100	0.00020800	-1.1001
125	0.00044013	-1.1078

3.7.2. Open circuit potentials

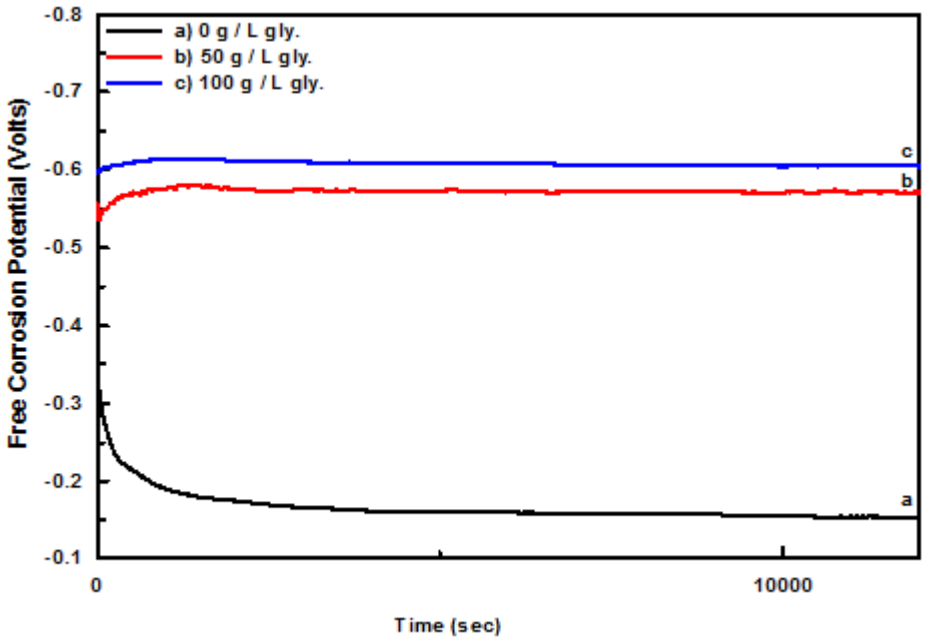

Figure 25. Free corrosion potentials vs. time for nickel deposited from glycine-free (a) and from glycine-containing (b,c) solutions in 3.5% NaCl .

Fig. 25 shows the time variations of the free corrosion potential for nickel deposited from glycine- containing solutions and from glycine –free solution in 3.5% NaCl solution in open circuit conditions. The data reveal that the nickel deposited from glycine- free solution (curve a) posses nobler potentials than that which deposited from glycine-containing solutions (curves b,c), which means that nickel deposited from glycine-containing bath posses a lower corrosion resistance than that without glycine. This result is in good agreement with the result obtained from the anodic polarization measurements. All of the samples tested reached the equilibrium potential within the time range of the measurements (approximately 4 h). To the best of our knowledge, no previously published reports refer to the corrosion resistance of nickel deposited from glycine solutions.

4. CONCLUSIONS

Addition of glycine to the nickel plating solution leads to:

- Improve the appearance of the nickel deposits, it becomes bright.
- Formation of a complex between nickel and glycine which depends strongly on pH as confirmed by the electronic spectra measurements.
- Glycine accelerates the Ni^{2+} ions reduction as confirmed by the polarization curves, the ALSV and CV.
- Decrease the throwing power, throwing index and Wagner number.
- Increase the degree of noncrystallinity, as shown by XRD analysis.

- Decrease the corrosion resistance of the nickel deposits.
- The formation of finer grains and the appearance of fine microcracks.

References

1. M. Saitou, T. Chinen and Y. Odo, *Surf. Coat. Technol.,* 115 (1999) 282.
2. U.S. Mohanty, B.C. Tripathy, P. Singh and S.C. Das, *J. Electroanal.Chem.,* 526 (2002)63.
3. M. Ga´lova´ , R. Orinˇa´kova´ and L. Lux, *J. Solid State Electrochem.,* 2(1998) 2.
4. R. Orinakova, A. Turonova, D. Kladekova, M. Galova and R. M. Smith, *J. Appl. Electrochem.,* 36 (2006) 957.
5. M. A. M. Ibrahim, S. S. Abd El Rehim, S. M. Abd El Wahaab and M. M. Dankeria, *Plat. Surf. Finish.,* 86(4) (1999) 69.
6. O. A. Taranina, N. V. Evreinova, I. A. Shoshina, V. N. Naraev, and K. I. Tikhonov, *Russ. J. Appl. Chem.,* 83(1) (2010) 58.
7. N. V. Sotskaya and O. V. Dolgikh, *Prot. Met.***,** 44(5) (2008) 479.
8. E. Rudnik, M. Wojnicki and G.Wloch, *Surf. Coat. Technol.,* 207 (2012) 375.
9. J. Lee a, W. Chung , U. Jung and Y. Kim , *Surf. Coat. Technol.,* 205 (2011) 4018.
10. M. A. M. Ibrahim, *J. Appl. Electrochem*., 36(2006) 295 .
11. E. M. Oliveira, G. A. Finazzi and I. A. Carlos, *Surf. Coat. Technol.*, 200 (2006) 5978.
12. A. Ciszewski, S. Posluszny, G. Milczarek and M. Baraniak, *Surf. Coat. Technol*. 183 (2004)127.
13. M. A. M. Ibrahim and S. N. Alamri, *J. Appl. Surf. Finish.,* 2(4) (2007) 332.
14. R. Tarozaite, A. Sudavicius, Z. Sukackiene and E. Norkus, *Trans. IMF,* 92(3) (2014)146.
15. M. A. M. Ibrahim and R. M. Al Radai, Mat. Chem. Phys., 151 (2014) 222.
16. M. H. Gharahcheshmeh and M. H. Sohi, *J. Appl. Electrochem.,* 40 (2010)1563.
17. S.I. Berezina, R.M. Sageeva, L.G. Sharapova, *Prot. Met.*, 86 (1986) 228.
18. J.C. Wei, M. Schwartz, K. Nobe, *J. Electrochem. Soc.*, 155 (2008) D660.
19. T. Boiadjieva, D. Kovacheva, L. Lyutov, M. Monev, *J. Appl. Electrochem.,* 38 (2008) 1435.
20. N.V. Evreinova, I.A. Shoshina, V.N. Naraev, K.I. Tikhonov, *Russ. J. Appl. Chem.,* 81 (2008) 1180.
21. U. Lačnjevac, B. M. Jović and V. D. Jović, *J. Electrochem. Soc.,* 159 (5) (2012) D310.
22. M.A.M. Ibrahim, *J. Appl. Surf. Finish.,* 3(2) (2008) 89.
23. S. Field, *Metal Ind.* (London), 44 (1934) 416.
24. M.A.M. Ibrahim, S.S. Abd El Rehim, M.M. El Naggar and M.A. Abbass, *J. Appl. Surf. Finish., **1***(4) (2006) 293.
25. M. Schwartz, N. V. Myung, and K. Nobe, *J. Electrochim. Soc*., 151 (7) (2004) C468.
26. F.M. Takata, P.T.A. Sumodjo, *Electrochim. Acta*, 52 (2007) 6089.
27. I. Mizushima, M. Chikazawa and T. Watanabe, J. *Electrochem. Soc*., 143(6)(1996)1978.
28. M. A. M. Ibrahim: *J. Chem. Technol. Biotechnol.,* 75 (2000) 745.
29. A.E. Mohamed, S. M. Rashwan, S. M. Abdel-Wahaab and M. M. Kamel, *J. Appl. Electrochem.,* 33(11) (2003)1085.
30. S.S. Abd El Rehim, S.M. Abd El Wahaab, S.M. Rashwan and Z.M. Anwar, *J. Chem. Technol. Biotechnol*., 75, (2000) 237.
31. C. Karwas and T. Hepel, *J. Electrochem. Soc*., 135 (1988) 839.
32. J. Horkan, *J. Electrochem. Soc*., 126 (1979) 1861.
33. S.S. Abd EL Rehim, M.A.M. Ibrahim and M.M. Dankeria, *J Appl. Electrochem.,* 32 (2002) 1019.
34. G. Trejo, A.F. Gil, I. Gonzalez, *J. Appl. Electrochem*., 26 (1996)1287.
35. B. Scharifker, G. Hills, *Electrochim. Acta,* 28 (1983) 879.

36. B. Scharifker, J. Mostany, M. Palomar-Pardave , I. Gonzalez, J. *Electrochem. Soc.*, 146 (1999)1005 .
37. G. Gunawardena, G. Hills, I. Montenegro, B. Scharifker, J. *Electroanal.Chem.***,** 138, (1982) 225.
38. C. Wagner, J. Electrochem. Soc., 98 (1951)116.
39. S.L. Marshall and S.K. Walf, *Electrochim. Acta*, 43 (1998)405.
40. C.T.J. Low, E.P.L. Roberts and F.C. Walsh, *Electrochim. Acta* 52 (2007) 3831.
41. S.S. Abd El Rehim, M.A.M. Ibrahim, M.M. Dankeria and M. Emad, *Trans IMF*, 80(3) (2002)105.